AED R-3601F
Issued: July 10, 1970

Fourth Quarterly Report Study to Determine and Improve Design for Lithium-Doped Solar Cells

Prepared for
Jet Propulsion Laboratory
California Institute of Technology
Pasadena, California
In fulfillment of
Contract No. 952555
April 1 to June 30, 1970

Prepared by
G. Brucker, T. Faith,
J. Corra, and A. Holmes-Siedle

RCA

RCA Corporation | Defense Electronic Products
Astro Electronics Division | Princeton, New Jersey

AED R-3601F
Issued: July 10, 1970

Fourth Quarterly Report Study to Determine and Improve Design for Lithium-Doped Solar Cells

Prepared for
Jet Propulsion Laboratory
California Institute of Technology
Pasadena, California
In fulfillment of
Contract No. 952555
April 1 to June 30, 1970
Prepared by
G. Brucker, T. Faith,
J. Corra, and A. Holmes-Siedle

RCA Corporation | Defense Electronic Products
Astro Electronics Division | Princeton, New Jersey

This work was performed for the Jet Propulsion Laboratory, California Institute of Technology, as sponsored by the National Aeronautics and Space Administration under Contract NAS 7-100.

PREFACE

This is the Fourth Quarterly Report on a program for a "Study to Determine and Improve Design for Lithium-Doped Solar Cells." This report was prepared under Contract No. 952555 for Jet Propulsion Laboratory, Pasadena, California, by the Astro-Electronics Division of RCA, Princeton, New Jersey. The preparation of this report is a contractual requirement covering the period from April 1 to June 30, 1970. The work reported here was conducted by the Radiation Effects group, Manager, Dr. A. G. Holmes-Siedle, of AED, which is located at the RCA Space Center. The Project Supervisor is Dr. A. G. Holmes-Siedle and the Project Scientist is Dr. G. J. Brucker. The Technical Monitor of the program is Mr. Paul Berman of the Solar Power group, Jet Propulsion Laboratory.

ABSTRACT

This is the Fourth Quarterly Report on a program to study and analyze the action of lithium in producing a recovery or spontaneous annealing of radiation damage in bulk silicon and silicon solar cells at room temperature or below. This program has technical continuity with the work performed by AED of RCA for JPL on Contract No. 952249. The eventual goal of this effort is to understand the damage and recovery mechanisms so that an optimum set of solar-cell design rules can be specified.

The test vehicles used for this work are (1) a group of solar cells supplied by JPL, and (2) silicon bars in the "Hall-bar" configuration. The source of particle irradiation being used is a 1-MeV electron beam produced by the RCA Laboratories Van de Graaff generator.

The present work has led to the formulation of a set of design rules and the construction of a matrix table listing solar cell parameters and their interrelations. These parameters were divided into three categories (1) fabrication, (2) initial cell parameters, and (3) dynamic and stability parameters. A fourth set of parameters, namely, the flight environment, also affects the dynamic and stability parameters. Environmental conditions such as temperature, particle flux, energy, and type of particle must ultimately be considered.

Performance and stability tests have been run at room temperature for periods ranging up to 550 days on p/n lithium solar cells and 10 Ω-cm non-lithium n/p control cells irradiated by 1-MeV electrons to fluences from 1×10^{14} to 3×10^{15} e/cm^2. Cold finger experiments have been performed to obtain information on lifetime damage constants over a bombardment temperature range from 80°K to 350°K and on cell recovery dynamics over an annealing temperature range from 280°K to 380°K. Quartz-crucible lithium cells have remained stable at generally competitive power levels after long recovery times (several months). Oxygen-lean lithium cells have shown two main types of instability after fast (hours to days) recovery times: (1) post-recovery short-circuit current redegradation which stabilizes after a ~ 100 day redegradation time, (2) radiation-independent open-circuit voltage loss, due to carrier depletion in the base region, which continues over a ≈ 500 day period. The activation energy for cell recovery was measured to be 0.66 eV in oxygen-lean silicon cells and 1.1 eV in crucible cells, equal to the activation energy for lithium diffusion in oxygen-lean and crucible silicon, respectively. Recovery rates in both types of cells were proportional to the lithium density gradient, dN_L/dw, measured before irradiation.

The measurements of Hall bars fabricated from quartz-crucible and float-zone silicon doped with lithium from 2×10^{14} to 2×10^{16} Li/cm^3 have proved successful, and have provided the data required to formulate a qualitative description of the damage and annealing mechanisms that take place in the lithium-oxygen-defect complex in silicon irradiated by 1-MeV electrons. Defects located at energies of ≈ E_c - 0.18 eV and

E_c - 0.13 eV were measured in quartz-crucible silicon of moderate resistivity (2×10^{15} Li/cm^3) bombarded by electrons at temperatures from 78°K to 200°K. Both of these defects anneal at room temperature (300°K) by the interaction of lithium with the defects. Results suggest that the rate of carrier-removal measured at high temperatures ($T_M \gtrsim 160$°K) increases with decreasing lithium concentration; thus, the lithium-oxygen complex reduces the production rate of the A-center. Annealing measurements made on quartz-crucible Hall bars indicate that several competing processes take place during the post-bombardment period. The short term results can not be explained on the basis of a single or a double lithium ion neutralizing a defect. Over a long period of time following bombardment, the results can be explained as due to a multiple complexing by many lithium ions at a defect center so as to produce an uncharged complex. A damage and annealing model was proposed based on the results obtained during a year of contractual effort.

The data from Hall measurements on bulk silicon and from solar-cell device measurements are in excellent agreement and allow some firm conclusions on optimum solar-cell design for space use.

CONTENTS

CONTENTS (Continued)

ILLUSTRATIONS

SECTION I

INTRODUCTION

A. GENERAL

This contract effort represents an experimental investigation of the physical properties of lithium-containing p-on-n solar cells and bulk silicon samples, and of the processes which occur in these devices and samples before and after irradiation. The program objectives are to develop and reduce-to-practice analytical techniques to characterize the radiation resistance of lithium-doped solar cells and its dependence on the materials and processes used to fabricate them. On the basis of these and other data, AED will determine and recommend an improved design of lithium-doped solar cells for space use. A previous RCA program (Contract No. 952249) performed for JPL provided the groundwork for this effort. Unless otherwise mentioned, the source of all irradiations was the 1-MeV electron beam of the RCA Laboratories Van de Graaff generator.

B. TECHNICAL APPROACH

The approach to the objectives is based on the irradiation and measurement of the electrical properties of bulk-silicon samples, government-furnished (GFE) solar cells, and in-house fabricated test-diodes. Experiments on bulk samples are to include Hall and resistivity measurements taken as a function of (1) bombardment temperature, (2) resistivity, (3) fluence, (4) oxygen concentration, and (5) annealing time at room temperature. Diffusion length measurements on solar cells and test diodes are to be made as a function of the same five parameters as for bulk samples. In addition, capacitance and I-V measurements are to be made on selected cells. Stability studies are to be conducted on solar cells, which will be irradiated and observed for long periods of time. Based on these results, a set of preliminary design rules and specifications will be determined, and solar cells will be procured by JPL in accordance with these rules. As a check of the validity of the design rules, tests will be conducted on this group of cells and a set of modified design rules will be derived.

C. SUMMARY OF PREVIOUS WORK

Some overall conclusions of the last reporting period were as follows: the low-temperature measurements of Hall bars and of solar cells proved very successful and provided some fruitful insights into the processes occurring in lithium-containing silicon. Correlation of lifetime damage constant K_τ with the carrier-removal rates, measured as a function of bombardment temperature ($\approx$80°K to 200°K), was experimentally demonstrated.

Long-term stability tests at room temperature on lithium-containing crucible-grown cells continued to show these cells to be stable for periods ranging up to 450 days. Most of the crucible cells which have completed their recovery cycles were competitive in power with commercial 10 ohm-cm n/p cells irradiated to the same fluence. For a fluence of 3×10^{14} e/cm^2, the time-to-half-recovery, θ, of these cells with the exception of T2, T7, and Sb-doped cells was related to the lithium density gradient dN_L/dw, through $\theta\ dN_L/dw = 6.5 \pm 2.5 \times 10^{20}$ days/cm^4 for $10^{18} \lesssim dN_L/dw \lesssim 5 \times 10^{19}$ cm^{-4}. The T2 and T7 cells' recovery rate is faster by a factor of $\sim 10^3$ while the Sb-doped cell recovery rate is much slower. Although many of the float-zone and Lopex cells suffered redegradation, some groups of Lopex cells, notably T6(1) and H7(1), ($\phi = 3 \times 10^{14}$ e/cm^2) were competitive with commercial n/p cells approximately 7 months after irradiation.

Cold finger experiments were performed on three (C6C) crucible cells with low lithium density gradient, $dN_L/dw \approx 10^{18}$ cm^{-4}, and two T9 Lopex cells with high lithium density gradient, $dN_L/dw \approx 5 \times 10^{19}$ cm^{-4}. Bombardment temperature, T_B, dependence of lifetime damage constant, K_τ, was measured. Both types of cells displayed a saturation of K_τ at high T_B and a decrease at lower temperatures in agreement with results previously obtained from carrier removal experiments on Hall samples. K_τ saturated at $T_B = 120°$K for the T9 cells and at $T_B \approx 105°$K for the C6C cells. The saturation values of K_τ, for a measurement temperature, T_M, of 200°K were $\approx 1.5 \times 10^{-7}$ cm^2/e-sec for C6C cells and $\approx 1.5 \times 10^{-6}$ cm^2/e-sec in the more heavily doped T9 cells. The damage constant for $T_B = T_M = 353°$K for the C6C cells was $\approx 1.3 \times 10^{-8}$ cm^2/e-sec, somewhat above the $\approx 8 \times 10^{-9}$ cm^2/e-sec value for 1 ohm-cm p/n cells at room temperature. Recovery rate measurements versus annealing temperature showed the activation energy for recovery in the C6C cells to be ≈ 1.1 eV which is the activation energy for lithium diffusion in crucible-grown silicon, and that for T9 cells to be ≈ 0.65 eV, the activation energy for lithium diffusion in silicon with low-oxygen content. The defect activation energy in the irradiated C6C cells, obtained for lifetime versus temperature measurements, was found to be ≈ 0.13 eV. No significant change in this level was observable after cell recovery.

Diffusion constant measurements made on a quartz-crucible cell (C6C20) show an activation energy of 1.03 eV indicative of dissociation of $Li0^+$ and diffusion of Li^+.

Hall and resistivity measurements on samples of float-zone silicon doped with lithium to concentrations of 2 to 5×10^{14} Li/cm^3 and bombarded by electrons indicated the production of a defect located in the forbidden energy gap at an energy of 0.12 eV below the conduction band. This defect was produced at bombardment temperatures ranging from 78°K to 200°K. Annealing of these samples at a temperature of 100°C did not remove the defect completely, although the concentration was reduced. These lightly doped samples exhibited annealing properties and carrier-removal rates ($\Delta n/\Delta\phi = 0.1$ cm^{-1} at $T_B = 100°$K to 200°K) which are similar to those of heavily doped (2×10^{16} Li/cm^3) quartz-crucible Hall bar samples. The results of the Hall bar experiments suggested that the ratio of oxygen to lithium concentration is an important parameter in determining the annealing properties in lithium-doped silicon. These properties include the stability of both the lithium neutralized and unannealed defect centers, and also the carrier-removal rate for high bombardment temperatures ($T_B = 100°$K to 200°K).

SECTION II

LONG-TERM PERFORMANCE OF JPL-FURNISHED CELLS

A. GENERAL

A large group of lithium-containing p/n silicon solar cells, manufactured by Centralab, Heliotek, and Texas Instruments, and some 10 ohm-cm commercial p/n cells were irradiated by 1-MeV electrons from a Van de Graaff generator at a rate of $\approx 4 \times 10^{13}$ e/cm^2-min to one of the following fluences: 1×10^{14}, 3×10^{14}, $5 \times 10^{14*}$, or 3×10^{15} e/cm^2. The cells were stored in the dark at room temperature and all irradiations were performed at room temperature. Measurements of cell photovoltaic characteristics have been made periodically with illumination by a 140 mW/cm^2 tungsten light source with long term reproducibility within 2 percent. Test durations range up to 550 days after irradiation. Periodic reverse-bias capacitance measurements (Ref. 1) of donor density profiles were made on many of the cells and electron-voltaic (Ref. 2) diffusion length measurements were made before and immediately after irradiation.

B. N/P CELL RECOVERY

Significant recovery occurred in the 10 ohm-cm n/p stored at room temperature after irradiation. Such recovery was observed in all 22 irradiated n/p cells, with most of the recovery occurring during the first 10 days after irradiation. This surprising degree of room temperature recovery, averaging $\approx$ 8 percent is an important factor in comparison with lithium cells and should prompt further investigation of n/p cell recovery near room temperature.

C. QUARTZ-CRUCIBLE CELLS

Physical properties of the QC (Li) cells and comparisons between the outputs of the QC (Li) cells and simultaneously irradiated 10 ohm-cm n/p cells are given in Table I, which is divided into three parts according to fluence: (a) $\phi = 1 \times 10^{14}$ e/cm^2, (b) $\phi = 3$ to 5×10^{14} e/cm^{2*}, and (c) $\phi = 3 \times 10^{15}$ e/cm^2. In each part the cells are listed in order of increasing speed of recovery, the group showing slowest recovery being first. Columns 1 and 2 list cell groups and the number of cells in each group, column 3 gives the initial dopants, and column 4 lists the (approximate) initial lithium density gradient. Columns 5 to 10 give maximum powers averaged

---

* In one such irradiation, the cells were erroneously exposed to $\approx 8 \times 10^{14}$ e/cm^2 of $\approx$ 0.7 MeV electrons.

TABLE I. PROPERTIES AND PERFORMANCE OF CRUCIBLE-GROWN LITHIUM CELLS AND COMPARISONS WITH COMMERCIAL 10 ohm-cm n/p CELLS

Cell Group	No. of Cells	Dopant	dN_L/dw (cm^{-4})	Cell Power (mW)						T.A.B. (days)
				Initial		After Irrad.		Latest Reading		
				Li cell	n/p	Li cell	n/p	Li cell	n/p	
(A) Low Fluence, 1×10^{14} e/cm^2										
C2 (1)	5	Sb	$1x10^{18}$	30.3	28.1	17.9	21.3	21.4	23.3	551
C1 (1)	7	As	$1x10^{18}$	30.3	28.1	18.6	21.3	24.6	23.3	551
H2 (1)	9	P	$1x10^{19}$	26.0	28.1	17.0	21.3	23.6	23.3	551
H1 (1)	8	As	$2x10^{19}$	21.7	28.1	15.7	21.3	20.2	23.3	551
(B) Intermediate Fluence, 3 to 5×10^{14} e/cm^2										
C2 (2)	2	Sb	$1x10^{18}$	30.3	27.7	14.8	17.7	15.7	18.9	483
C6A (1)	3	Sb	$1x10^{18}$	28.2	28.2	15.1	19.5	15.5	20.9	266
C6B (1)	3	Sb	$1x10^{18}$	29.3	28.2	15.7	19.5	17.0	20.9	266
C6C (1)	3	P	$1x10^{18}$	28.1	28.2	16.0	19.5	17.4	20.9	266
C5 (5)	3	P	$1x10^{18}$	30.9	28.2	16.6	19.5	18.7	20.9	266
*C1 (2)	2	As	$1x10^{18}$	31.8	28.4	13.8	16.6	16.9	18.9	483
T8 (1)	3	P	$1x10^{19}$	26.1	28.2	12.6	19.5	19.4	20.9	266
H2 (2)	2	P	$1x10^{19}$	24.3	27.7	13.5	17.7	20.0	18.9	483
H6 (1)	3	P	$1x10^{19}$	24.7	28.2	14.0	19.5	21.3	20.9	483
*H1 (2)	2	As	$2x10^{19}$	17.4	28.4	10.8	16.6	15.8	18.9	483
C5 (1)	3	P	$5x10^{19}$	25.0	28.2	13.0	19.5	20.7	20.9	266
(C) High Fluence, 3×10^{15} e/cm^2										
C2 (3)	2	Sb	$1x10^{18}$	30.1	28.4	10.7	13.9	10.9	15.6	483
C6A (2)	3	Sb	$1x10^{18}$	28.9	28.3	9.7	14.2	9.8	15.6	266
C6B (2)	3	Sb	$1x10^{18}$	28.9	28.3	10.1	14.2	10.1	15.6	266
C6C (2)	3	P	$1x10^{18}$	28.3	28.3	10.7	14.2	10.7	15.6	266
C5 (6)	3	P	$1x10^{18}$	28.4	28.3	11.0	14.2	11.2	15.6	266
T8 (2)	3	P	$1x10^{19}$	26.1	28.3	8.5	14.2	9.9	15.6	266
H6 (2)	3	P	$1x10^{19}$	20.9	28.3	9.5	14.2	12.1	15.6	266
H2 (3)	3	P	$1x10^{19}$	25.2	28.4	9.9	13.9	15.2	15.6	483
C5 (2)	3	P	$5x10^{19}$	25.1	28.3	8.2	14.2	15.1	15.6	266

T.A.B indicates time after bombardment at latest reading.
* $\omega \approx 8 \times 10^{14}$ e/cm^2 of ≈ 0.7 MeV electrons

over the cell groups, columns 5, 7, and 9 for the lithium cells before irradiation, immediately after irradiation, and at the latest reading, respectively; columns 6, 8, and 10 give the equivalent values for the n/p cell groups. Column 11 gives the time after bombardment at the latest reading.

Several of the QC (Li) cell groups have initial powers comparable to or above the n/p cells, cf, columns 5 and 6. Immediately after irradiation (columns 7 and 8), the p/n lithium cells show greater damage. This is as expected because the damage introduction rate in n-type silicon is greater than that in p-type silicon. However, these columns which indicate the radiation resistance in the absence of lithium diffusion have little practical meaning since radiation to the fluences employed in these experiments would accrue only after orbit durations of ~1 year during which damage and recovery would occur simultaneously. The latest readings (columns 9 and 10) are of greater practical interest. Of the four lithium cell groups irradiated to 1×10^{14} e/cm^2, two [C1 (1) and H2 (1)] have recovered to powers greater than the recovered n/p values. Group C2(1) is below the n/p level; however, the C2(1) cells are still recovering. The C2, C6A, and C6B cells which were made from silicon doped with antimony have all shown the surprisingly slow recovery previously reported (Ref. 3) suggesting that Sb-doping inhibits the diffusion of lithium. Eleven lithium cell groups, irradiated to fluences of 3 to 5×10^{14} e/cm^2, are listed in Table I(b). The recovery times become longer with increasing fluences due to the greater loss of lithium during irradiation. Consequently, none of the cell groups with density gradients below 10^{19} cm^{-4} have recovered to the n/p power levels. Of the cells which have recovered, groups H2(2), H6(1), and C5(1) are competitive with the n/p cells. Groups T8(1) and C1(2) are not yet competitive but are still recovering. Of the eleven cell groups irradiated to 3×10^{15} e/cm^2, the first five groups with low density gradient (10^{18} cm^{-4}) have yet to recover. Two groups H2(3), and C5(2), $dN_L/dW > 10^{19}$ cm^{-4} have recovered to power levels competitive with the n/p cells. At the present time, the lithium cell group with the best competitive position is group C1(1) with an averaged power of 24.6 mW, approximately five percent above the recovered n/p level.

The quartz-crucible cells have shown good stability. No instance of either post-recovery redegradation of irradiated cells has occurred in times ranging up to 550 days.

D. OXYGEN-LEAN CELLS

Table II lists the properties and performance of the irradiated groups of oxygen-lean cells. Column 1 lists the cell groups, L or F after the group code designating Lopex* or float-zone cells. Column 2 gives the number of cells in the group. Column 3 gives the lithium density gradient, the cell groups being listed in order of increasing gradient. Columns 4 through 7 give the cell powers before irradiation, immediately

* Trademark of Texas Instruments Corporation.

TABLE II. PROPERTIES, PERFORMANCE, AND STABILITY OF FLOAT-ZONE AND LOPEX LITHIUM CELLS

Cell Group	No. of Cells	dN_L/dw (cm^{-4})	Initial	Cell Power (mW)			T.A.B.** (Days)	% Redegradation
				After Irrad.	Receovered	Latest Reading		
(A) Low Fluence, $1x10^{14}$ e/cm^2								
C4(9) F	4	$1x10^{18}$	21.1	16.6	21.1	20.0	483	5
T2 (1)___	6	$3x10^{18}$	26.8	16.5	23.6	23.4	549	1
C4 (17) F	4	$3x10^{18}$	19.6	16.0	19.5	18.5	483	5
C4 (5) F	4	$2x10^{19}$	17.7	15.3	17.4	16.0	483	8
C4 (13) F	4	$4x10^{19}$	15.0	13.6	14.4	13.6	483	6
C4 (1) F	3	$5x10^{19}$	15.8	14.2	15.3	14.0	483	8
T3 (1) L	3	$2x10^{20}$	*(61.6)	(45.8)	(57.7)	(53.5)	483	(8)
(B) Intermediate Fluence 3 to $5x10^{14}$ e/cm^2								
H5 (1) F	3	$<10^{17}$	28.7	12.3	13.8	13.8	266	0
C4 (10) F	3	$1x10^{18}$	20.3	12.1	17.9	17.6	483	2
C5 (7) F	3	$1x10^{18}$	21.6	11.2	17.8	17.8	266	0
C4 (18) F	3	$3x10^{18}$	20.8	12.7	19.5	19.1	483	2
C4 (6) F	3	$2x10^{19}$	17.5	12.1	16.7	15.6	483	7
H7 (1) L	3	$2x10^{19}$	24.1	13.8	22.0	21.1	266	4
T6 (1) L	3	$3x10^{19}$	26.8	12.1	21.0	21.0	266	0
T7 (1)___	3	$3x10^{19}$	25.2	10.8	19.4	18.7	266	4
C4 (14) F	3	$4x10^{19}$	15.3	12.6	14.7	13.9	483	6
‡C5 (3) F	3	$4x10^{19}$	17.5	13.3	16.1	15.5	266	4
C4 (2) F	3	$5x10^{19}$	15.8	12.2	14.8	13.8	483	7
T9 (1) L	3	$5x10^{19}$	26.9	10.9	21.1	19.6	170	7
T3 (2) L	3	$2x10^{20}$	*(60.4)	(30.5)	(46.7)	(42.2)	483	(10)
T4 (1) F	3	$2x10^{20}$	22.9	15.3	19.5	18.1	266	7
T5 (1) L	3	$3x10^{20}$	25.2	11.4	20.5	18.4	266	10
T10 (1) L	3	$3x10^{20}$	22.8	12.3	19.9	17.0	170	15
(C) High Fluence $3x10^{15}$ e/cm^2								
T2 (3)___	2	$3x10^{18}$	*(68.8)	(31.8)	(49.6)	(49.6)	483	(0)
C4 (19) F	3	$3x10^{18}$	20.0	8.7	12.3	12.3	483	0
C4 (7) F	3	$2x10^{19}$	17.7	8.1	14.3	14.3	483	0
H7 (2) L	3	$2x10^{19}$	22.8	8.5	15.5	15.5	266	0
T6 (2) L	3	$3x10^{19}$	*(69.6)	(24.5)	(49.7)	(49.7)	266	(0)
T7 (2)___	3	$3x10^{19}$	*(70.5)	(25.3)	—	—	266	(0)
‡C5 (4) F	3	$3x10^{19}$	16.6	9.5	13.6	13.6	266	0
C4 (15) F	3	$4x10^{19}$	15.1	9.5	13.4	13.2	483	1
T9 (2) L	3	$5x10^{19}$	26.6	6.5	14.5	14.5	170	0
C4 (3) F	3	$5x10^{19}$	15.3	9.1	13.4	12.7	483	5
T3 (3) L	3	$2x10^{20}$	23.1	7.9	14.7	13.9	483	6
T10 (2) L	3	$3x10^{20}$	*(56.5)	(22.3)	(36.2)	(34.5)	170	(5)
T4 (2) F	3	$3x10^{20}$	22.3	7.9	13.6	12.9	266	5
T5 (2) L	3	$4x10^{20}$	23.4	7.5	13.5	12.2	266	10

*Numbers in parentheses indiate short circuit current (mA)
‡5% Pre - Irradiation Degradation
**T.A.B - Time after bombardment to latest reading

after irradiation, at peak recovery, and as of the latest reading, the values listed being the average over the cells in the group. (The after-irradiation values in column 5 do not reflect the total damage during the irradiation since they were taken ≈15 minutes after irradiation ceased, i.e., after ≈15 minutes recovery time.) Column 8 gives the time after irradiation at the latest reading, and column 9 gives the percent power (or current) redegradation, measured from the peak recovered value, as of the latest reading. Cell groups from two cell lots, i.e., T2 and T7, came labelled as QC cells. However, both their rapid recovery ($\sim 10^3$ faster than QC cells) and their activation energy for recovery, measured to be ≈0.66 3V (see Figure 8) indicate that they are actually oxygen-lean cells. From column 7 of Table II it is seen that very few of these lithium cell groups have powers competitive with the n/p control cells (cf. column 10 of Table I). Only groups T2(1) with 23.4 mW (n/p power = 23.3 mW), T6(1), with 21.0 mW (n/p power = 20.9), and H7(2) with 15.5 mW (n/p power = 15.6 mW) are competitive with the recovered power levels of the commercial n/p cells. Column 9 indicates that most of the cell groups have suffered significant redegradation with greater redegradation generally suffered by groups with higher dN_L/dw.

Figure 1 shows time to peak recovery, θ_p, versus lithium donor density gradient, dN_L/dw, for the cell groups listed in parts (b) and (c) of Table II. The recovery rate after 3 to 5 x 10^{14} e/cm^2 and the lithium gradient show a fairly good linear relation over a lithium gradient range of ≈400. The relationship is $\theta_p \, dN_L/dw = 6(\pm 4) \times 10^{19}$ days/cm^4.

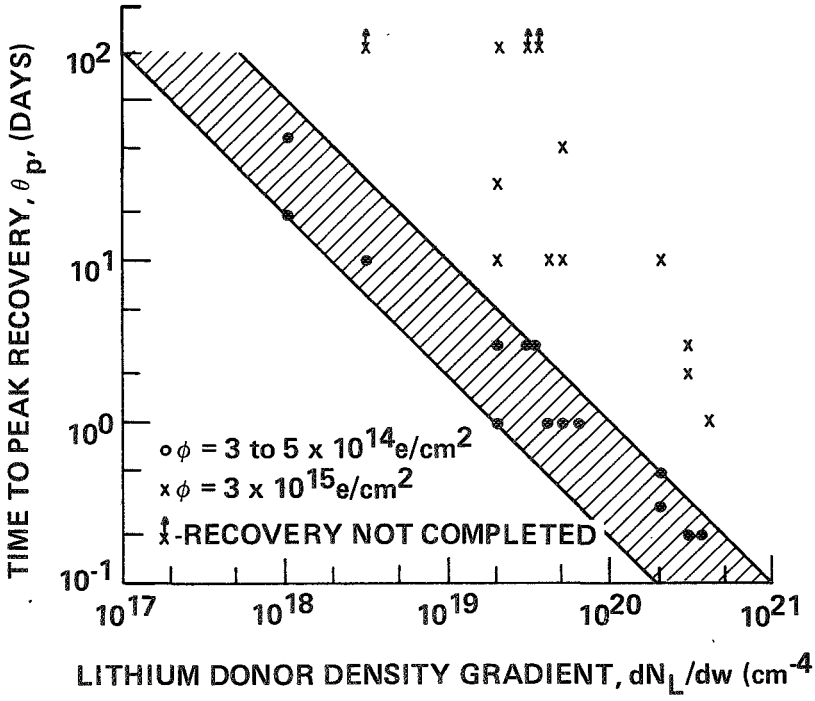

Figure 1. Time to Peak Cell Recovery vs Lithium Donor Density Gradient, Oxygen-Lean Cells

The values of θ_p are both higher and more spread out after the higher fluence of 3×10^{15} e/cm^2 due to the greater loss of lithium in defect formation at the higher fluence, leaving less free lithium near the junction to participate in cell recovery.

After a period of stability most of the cells start to redegrade. Figure 2 gives a logarithmic plot of the days after irradiation to a 2-percent power redegradation, θ_d vs lithium donor density gradient for the float-zone and Lopex cell groups irradiated to 3 to 5 x 10^{14} e/cm^2. The points with vertical arrows represent groups showing less than 2-percent redegradation as of the latest reading. The points are widely spread but show a definite trend toward decreasing time to redegradation with increasing lithium gradient, all of the points lying above and to the right of the line represented by $\theta_d \; dN_L/dw = 2 \times 10^{20}$ days/cm^4.

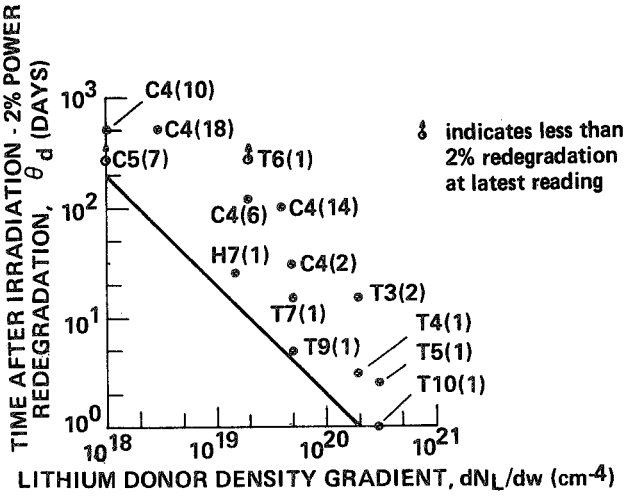

Figure 2. Time After Irradiation to the Onset of Two Percent Power Redegradation vs Lithium Donor Density Gradient, Oxygen-Lean Cells

Figure 3 employs the data of Figure 2 to plot the fraction of cell groups remaining stable versus the time-lithium gradient product. It is seen that half of the cell groups begin to suffer significant redegradation between 2 x 10^{20} and 10 x 10^{20} days/cm^4. Thus, only half of the cell groups remain stable at $\theta_d \; dN_L/dw = 10 \times 10^{20}$ days/cm^4, i.e., half the groups remain stable for a duration greater than ten times the time to full recovery, $\theta_r \; dN_L/dw = 6 \; (\pm 4) \times 10^{19}$ cm^{-4}.

There are, however, examples of good long-term stability, most notable among these is group T6(1), in which cell recovery occurs within the first three days, the subsequent decrease in short-circuit current being less than 2 percent over a period extending to 266 days after irradiation.

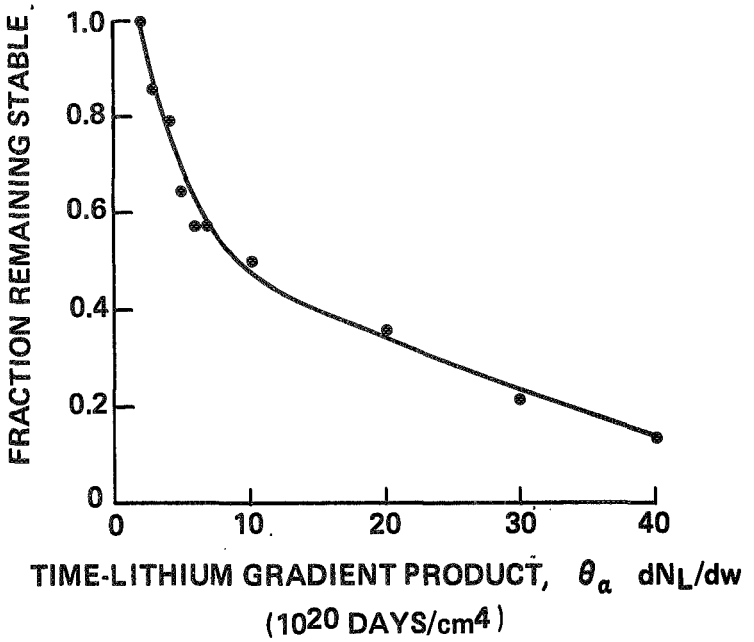

Figure 3. Fraction of Cells Remaining Stable vs Time-Lithium Gradient Product, Oxygen-Lean Cells

The mode of instability which has most often been observed is a redegradation in short-circuit current after recovery from irradiation. Stability tests on a large number of unirradiated cells indicate that it occurs only in irradiated cells; e. g., group T10(1) suffered 15-percent short-circuit current redegradation after recovery from 3×10^{14} e/cm^2 while group T10(3), from the same cell lot but unirradiated, suffered no loss in short-circuit current during the same time period. Most of the oxygen-lean cell groups suffered some redegradation by this radiation-dependent mode. After a period of redegradation via this mode, the cell outputs usually stabilize. Such stabilization is illustrated in Figure 4 which shows six cell groups that redegraded via the radiation-induced short-circuit current mode. In all groups, the largest part of the redegradation occurred during the first 25 days and all groups except T10(1) have been stable since the 100th day. Only groups H7(1) and T6(1) have powers competitive with the recovered n/p cell level of 20.9 mW. However, the apparent stabilization of the cells after a redegradation period suggests that oxygen-lean lithium cells can be made to be reliable and competitive with n/p cells.

Another type of instability, involving a loss in open-circuit voltage, V_{OC}, was observed in C4 cells. Capacitance measurements show this instability to be due to the loss of donors in the base region of the cell. Such losses have been observed in equal degrees in both irradiated C4 cells after recovery and in unirradiated C4 cells, this mode is, thus, not dependent on irradiation. It is, however, somewhat dependent on the lithium gradient, generally being more severe at higher dN_L/dw. An example of the time dependence of the V_{OC} degradation is given in Figure 5 in which V_{OC} is plotted against time for four of the most severely effected cells. The degradation is seen to continue even after $\approx$500 days. There are two possible explanations for the carrier loss near the junction that RCA is aware of: (1) motion of lithium ions toward the p-skin under the influence of the p/n junction electric field. Such lithium motion has

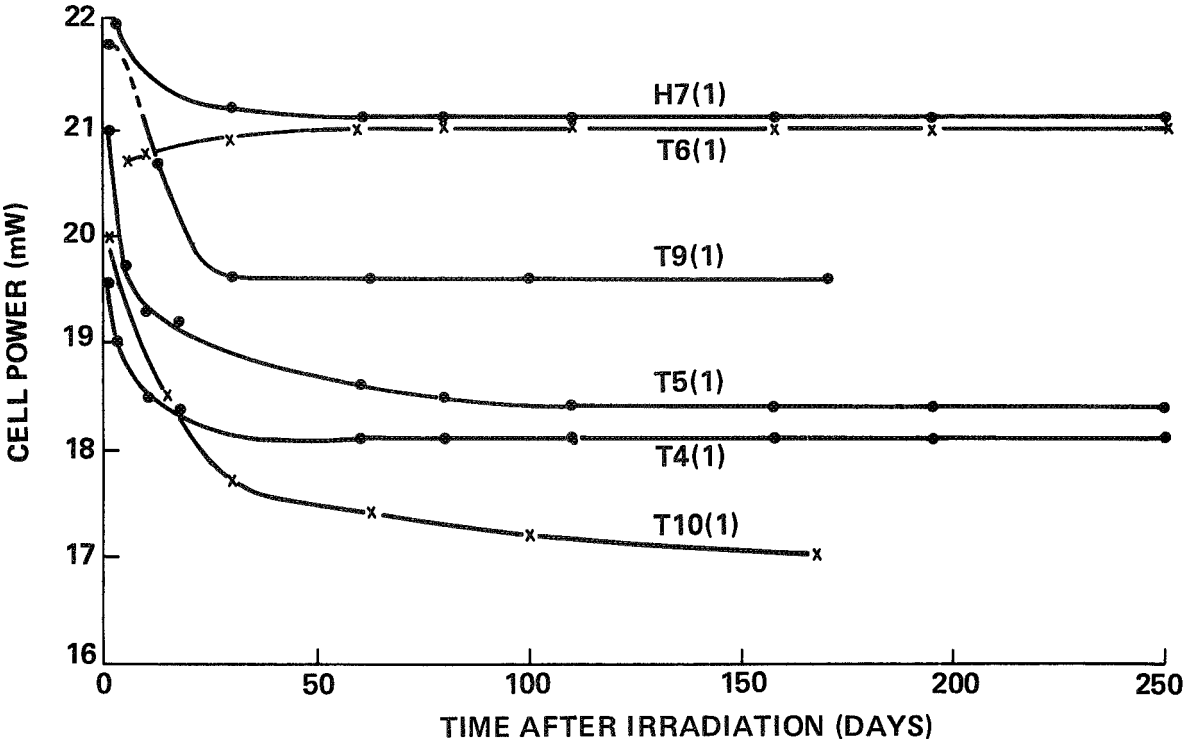

Figure 4. Cell Power vs Time After Irradiation, Oxygen-Lean Cells

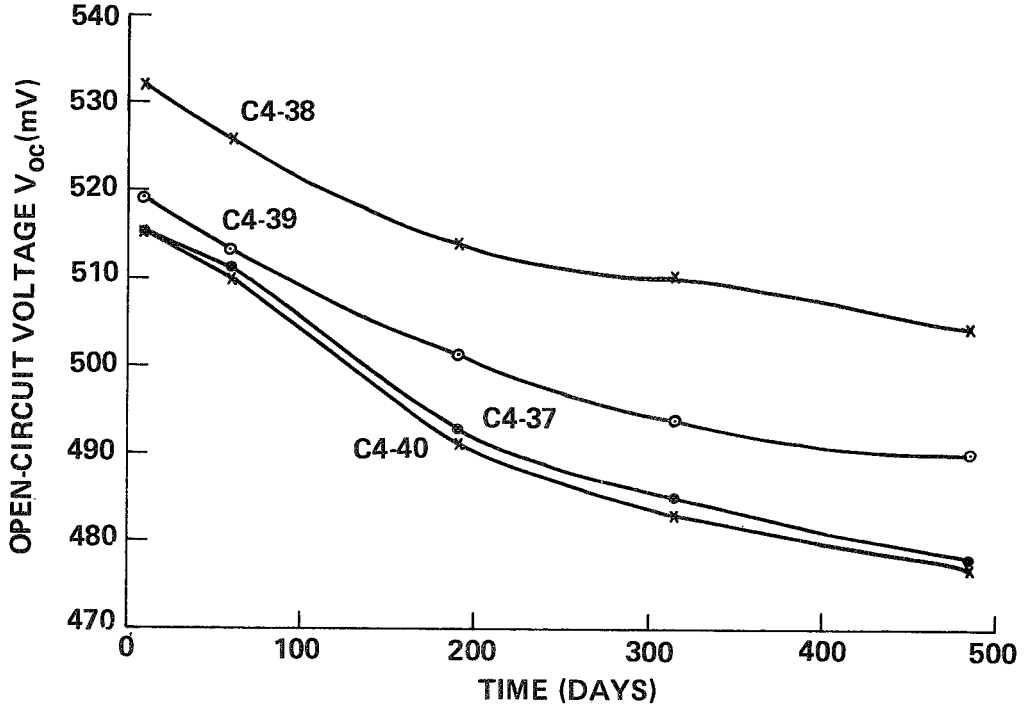

Figure 5. Open-Circuit Voltage vs Time, C4 Cells

previously been observed (Ref. 4); it resulted, however, in an increase in lithium donor density rather than a decrease, and (2) Precipitation of lithium into electrically inactive (uncharged) agglomerates. This is physically feasible since the lithium donor density in most lithium cells is greater than the solid solubility of lithium in silicon ($\sim 10^{14}$ cm^{-3}) at room temperature. However, if precipitation occurs in the C4 cells it is then a question why similar occurrences are not observed in the other lithium cells.

SECTION III

LITHIUM DIFFUSION CONSTANT

Lithium diffusion constant measurements have been continued using two high density gradient quartz-crucible cells (see Ref. 9). These particular cells (C5-19, C5-20) are very similar and have a lithium density at the junction edge (1.09 micrometers) of $\sim 8 \times 10^{14}$ Li/cm^3 and a density gradient of $\sim 5 \times 10^{19}$/cm^4 making these among the highest-density-gradient quartz-crucible cells received. Similar cells (C5(1)) have also shown a very predictable time to half recovery (I_{sc}) of 10 days when irradiated to 3×10^{14} 1-MeV elec/cm^2 (Ref. 5). In addition, these cells are competitive with n/p cells and have shown excellent stability. The lithium-ion diffusion constant was measured between 30°C and 64°C at 1.09 micrometers from the junction. The results are shown in Figure 6. Also shown in Figure 6 are the results of Pell (Ref. 6, 7, 8) for lithium diffusion constant in quartz-crucible silicon containing an oxygen concentration of about 10^{18} atoms/cm^3. Both measurements show excellent agreement indicating the presence of about 10^{18} atoms/cm^3 of oxygen in these cells at 1.09 micrometers from the junction. The 1.07 ev activation energy, as explained previously (Ref. 9), results from the dissociation of LiO^+ (~0.42 ev) into Li^+ and O and the subsequent diffusion of free (Li^+) lithium (~0.65 ev). The data shown in Figure 6 leaves little doubt that the recovery of high-density-gradient lithium-doped quartz-crucible cells is associated with the diffusion of free lithium (Li^+), as was already established firmly for cells of lower density gradient.

One difference between the present results and previous results (Ref. 9) is the better agreement with diffusion constant values obtained on bulk silicon.

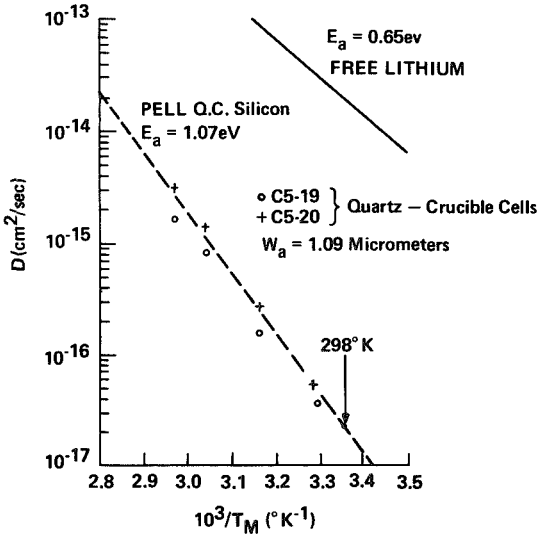

Figure 6. Diffusion Constant of Cells C5-19 and C5-20 vs Inverse Temperature

SECTION IV
SOLAR CELL EXPERIMENTS

A. GENERAL

The objectives of these experiments is to obtain information on: (1) dependence of lifetime damage constant, K_τ, on bombardment temperature, and (2) dependence of cell recovery rates and redegradation rates on annealing temperature in the temperature range from 280°K to 380°K.

The beam from the Van de Graaff was used for diffusion length measurements (Ref. 2), as well as for cell irradiation. Minority-carrier lifetime, τ, was obtained from the measured diffusion length, L, through the relation $L = \sqrt{D\tau}$, where D is the minority-carrier (hole) diffusion constant, and through use of the mobility data of Morin and Maita (Ref. 10) and the Einstein relation. Periodic measurements of diffusion length during electron irradiation enabled the calculation of lifetime damage constant, K_τ, using the equation

$$\frac{1}{\tau} = \frac{1}{\tau_{bb}} + K_\tau \phi \qquad (1)$$

where

τ_{bb} is the lifetime prior to irradiation, and

ϕ is the electron fluence.

B. LIFETIME DAMAGE CONSTANT

The results of these measurements are shown in Figure 7 where the measurement temperature, T_M, is 300°K. Since the density near the junction increases approximately linearly with distance from the junction, the cells are characterized in Figure 7 by the density gradient dN_L/dw. The cell diffusion length at T_M = 200°K was $\approx 20\,\mu$m during the measurements, therefore an approximate estimate for the average density in the current collection volume would be that $\approx 10\,\mu$m from the junction or $\approx 10^{-3}\ dN_L/dw\ (cm^{-3})$. The figure shows both oxygen-rich (QC) and oxygen-lean (FZ and Lopex) cells. The QC cells have saturated values of K_τ well below (a factor of $\approx$3) the FZ and L cells in agreement with the carrier removal results on bulk samples. The exponential decrease in K_τ at low temperatures and saturation at high temperatures is also in agreement with the carrier-removal results. The relative

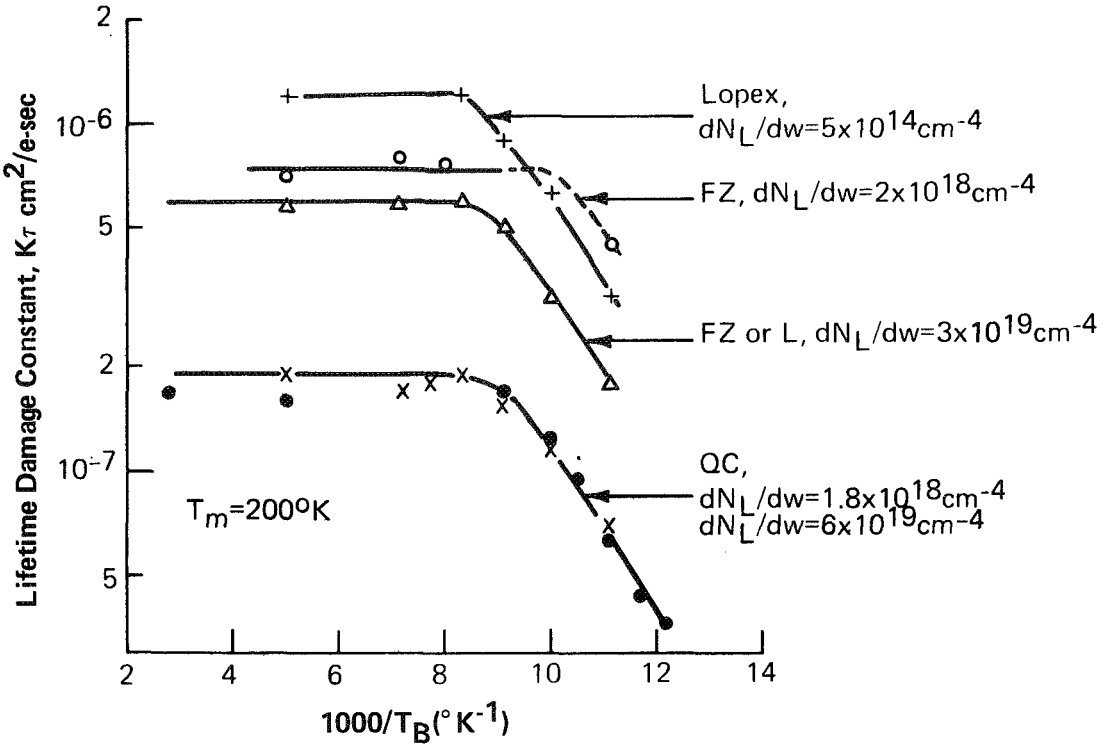

Figure 7. Lifetime Damage Constant vs Inverse Bombardment Temperature for Measurement Temperature of 200°K, Cell C6C-18(2)

insensitivity of the saturated value of K_τ to lithium density gradient is also evident. In oxygen-lean silicon the value of K_τ changes by ≈ 2 for a gradient change of ≈ 20. The change in oxygen-rich silicon is nil (within error) for cells differing in dN_L/dw by a factor of ≈ 30.

C. CELL RECOVERY

Successive anneals at different annealing temperatures, T_A, were performed on several oxygen-rich and oxygen-lean cells. During the anneal, the quantity $f_r^{-1} = e^{St}$, where $S = 4\pi r_o N_L D_L$ was plotted versus annealing time, where f_r^{-1} is reciprocal fraction of damage remaining, S is the recovery slope, r_o is the capture radius for lithium by the defect, N_L is the lithium density, and D_L is the lithium diffusion constant. The only quantity in S which is strongly temperature dependent is D_L. Thus, D_L can be calculated by finding S and inserting values for r_o and N_L. In Figure 8, plots of S versus inverse annealing temperature are given for QC cells with two different values of dN_L/dw. The solid lines drawn through the experimental points represent an activation energy of 1.07 eV, the activation energy (Ref. 7,8) for the diffusion of

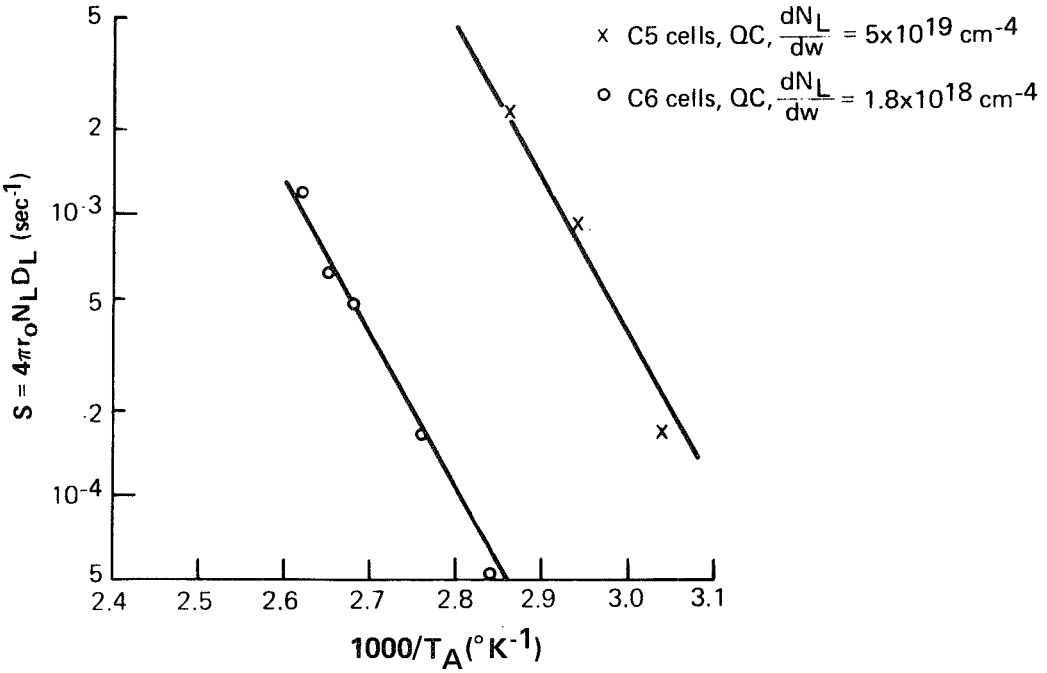

Figure 8. Recovery Slope vs Inverse Annealing Temperature (Recovery Activation Energy for Crucible-Grown Cells)

lithium in QC silicon. The values of D_L calculated from the data assuming $r_o = 10$ Å and $N_L = 10^{-3}\ dN_L/dw$ agree well with Pell's values for silicon containing an oxygen concentration of $\approx 5 \times 10^{17}$ cm^{-3}. This confirms that lithium diffusion to defect sites is responsible for recovery in lithium-containing QC cells.

The recovery curves for three groups of low oxygen content cells are given in Figure 9. The solid lines represent the 0.66 eV activation energy (Ref. 7, 8) for lithium diffusion in oxygen-lean silicon. Using $r_o = 10$ Å and $N_L = 10^{-3}\ dN_L/dw$, the values calculated from the data for D_L agree with Pell's within a factor of ≈ 2. It is noteworthy that the ratios of the values of S at a given value of T_A are (within a factor of 2) equal to the ratios of the lithium density gradients, dN_L/dw, measured in the cells. This is further indication that the quantity dN_L/dw is a reasonable index of recovery speed.

D. REDEGRADATION

Cells from lot T9 had shown considerable ($\approx$ 10%) redegradation of photovoltaic characteristic after recovery from irradiation. Therefore, they were chosen for redegradation studies on the cold finger. Anneals at various temperatures were carried

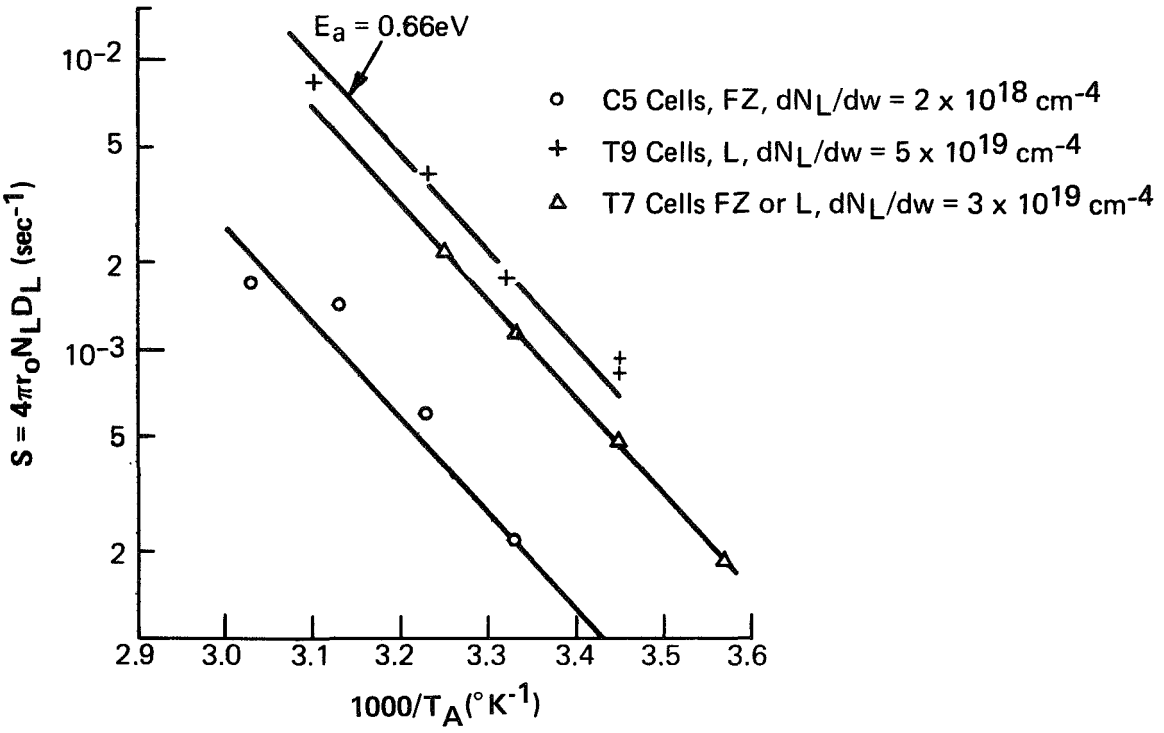

Figure 9. Recovery Slope vs Inverse Annealing Temperature (Recovery Activation Energy for Float-Zone and Lopex Cells)

out beyond the point of maximum recovery. The redegradation characteristic was thus observed as a function of annealing temperature. The results of the experiment are shown in Figure 10, which normalized lifetime is plotted versus annealing time for annealing temperatures of 357°K, 345°K, and 322°K. Plotted on the same coordinates is an annealing curve of normalized carrier density for an FZ Hall-bar sample at an annealing temperature of 300°K. Each of the curves rises to a peak (recovers) and then redegrades. The recovery and redegradation rates increase with increasing annealing temperature and all four redegradation curves show similar shape. The last fact indicates that there may be an effective activation energy for redegradation which is close to that for lithium diffusion in silicon.

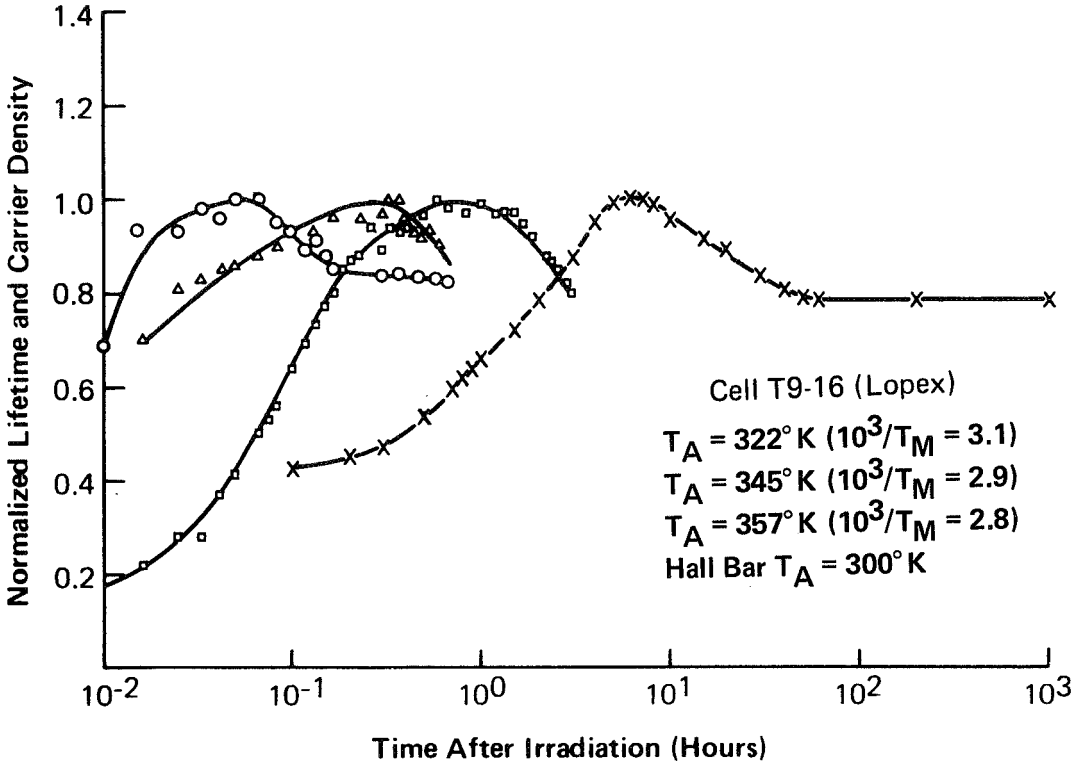

Figure 10. Normalized Lifetime and Carrier Density vs Annealing Time at 357°K, 345°K, 322°K, and 300°K

SECTION V

CELL MATRIX

A. CELL PARAMETERS

The parameters which determine and describe the physical properties and performance of the lithium cell can be divided into three sets: (1) fabrication parameters, (2) initial cell properties, and (3) dynamic and stability parameters. The fabrication parameters determine both of the other sets. However, a fourth set of parameters namely the flight environment also has strong influence on the dynamic and stability parameters which are deemed desirable. Environmental parameters such as cell temperature, particle flux, energy, and type of particle must ultimately be considered. In the present work, the radiation environment is a high flux of 1 MeV electrons over a short time span. The temperature is generally room temperature (stability experiments) with supplementary data from the solar cell (cold finger) experiments at temperatures up to 380°K.

While the set of environmental variables was limited by the nature of the experiment, these tests included a large number of cell parameters, many of which are listed in Tables I and II. A further breakdown of parameters according the three sets listed above follows:

(1) Fabrication parameters
   - (a) cell manufacturer
   - (b) silicon type (oxygen concentration)
   - (c) starting resistivity (ρ_o)
   - (d) starting n-type dopant (P, As, Sb)
   - (e) lithium source (paint on, evaporated)
   - (f) lithium diffusion/redistribution schedule

(2) Initial cell properties
   - (a) short-circuit current (I_{sc})
   - (b) open-circuit voltage (V_{oc})
   - (c) power (P)
   - (d) curve power factor (f)

(e) diffusion length (L)

(f) lithium donor density gradient (dN_L/dw)

(3) Dynamics and stability

(a) recovery speed

(b) redegradation speed

(c) short-circuit current redegradation

(d) open-circuit voltage instability

These parameters are listed vertically and horizontally in Table III, the matrix elements of which suggest the degree of interaction between the variables listed in the corresponding row and column. The letter S denotes a strong interaction; W, some interaction, but not so strong or well correlated; O, no interaction; a question mark (?), insufficient data to establish either an interaction or lack of same. A dash (—) indicates pairs of variables, which are by their nature independent.

Explanations for the more important elements in Table III are given below by rows starting with the first row.

Manufacturer:

V_{oc} redegradation (W): No T or H cells experienced

V_{oc} loss, however one C cell lot (C4) did. Most other C cells did have stable V_{oc}.

dN_L/dw (W): the T cells, taken as a group, had higher dN_L/dw than the C and H cells.

L, f, P, I_{sc} (S, S, W, S) T cells had higher I_{sc} and L, but lower f than C and H cells. The result was slightly higher initial power (for a given dN_L/dw) in the T cells.

Lithium source (S): T cells used evaporated lithium source: H and C cells (except H3A) used paint-on source. The question here is, could this factor contribute to the higher L values in T-cells. Several C and H cell lots using evaporated lithium source could answer this question.

Silicon Type:

The initial performance, recovery, and redegradation dynamics are strong functions of silicon type (oxygen content). This was discussed in Sections II and IV.

Starting Resistivity (ρ_o)

f(W): In some of the oxygen-lean cells with low dN_L/dw, f is poor (especially after irradiation) due to series resistance. Starting resistivities in the

TABLE III. LITHIUM SOLAR CELL PARAMETERS AND THEIR INTERRELATIONS

	V_{oc} instability	I_{sc} Redegradation	Redegradation speed	Recovery speed	dN_L/dw	L	f	P	V_{oc}	I_{sc}	Diff./Redist.	Li Source	Start. Dopant	ρ_o	Si Type
mfr.	W	O	O	O	W	S	S	W	W	S	—	S	W	O	W
Si type	S	S	S	S	W	S	O	S	O	S	—	—	—	W	
ρ_o	O	O	O	O	O	O	W	W	O	O	—	—	—		
Start. dopant	?	?	?	S	—	O	O	O	O	O	—	—			
Li source	O	O	O	O	?	?	?	?	O	?	—				
Diff/redist	W	S	S	S	S	S	O	S	S	S					
I_{sc}	O	O	O	O	S	S	O	S	W						
V_{oc}	O	O	O	O	S	W	O	S							
P	O	O	O	O	S	S	S								
f	O	O	O	O	O	O									
L	O	O	O	O	S										
dN_L/dw	W	S	S	S											
Rec. speed	W	S	S												
Redeg. speed	—	—													
I_{sc} redeg.	W														

Legend:

S = strong correlation
W = some correlation
O = no correlation
— = independent parameters

oxygen-lean cells have always been high (> 20 ohm-cm). It is suggested that a lower starting resistivity could avoid many series resistance problems.

Starting Dopant:

The effect of Sb-doping in reduction of recovery speed in QC cells has been observed. It would be interesting to test this effect in oxygen-lean cells.

Lithium Source:

Many interesting questions remain concerning the effect of the lithium source. To answer such questions, more H and C cells with evaporated lithium source must be tested. (Thorough tests on lot H3A, part evaporate and part paint-on, are being initiated.)

Lithium Diffusion/Redistribution:

dN_L/dw (S): The lithium gradient is strongly dependent on the lithium introduction schedule. In particular, increasing redistribution times give reduced dN_L/dw. However, for a given introduction schedule, large (factors sometimes > 5) cell-to-cell differences in lithium gradient are observed. The strong dependence of many of the performance and dynamic parameters on the introduction schedule is believed to be due to the resultant variations in dN_L/dw.

Lithium Donor Gradient (dN_L/dw):

The dependence of the dynamic and stability properties on dN_L/dw has been discussed in Sections II and IV. For a given manufacturer, L decreases with dN_L/dw.

Recovery Speed:

Redegradation speed (S): This relationship was also discussed in Sections II and IV.

B. MISSION COMPATIBILITY

The difference in the dynamics of oxygen-rich and oxygen-lean lithium cells is due to the factor of $\sim 10^3$ difference in the lithium diffusion constant, $D_L \approx 2 \times 10^{-17}$ cm^2/sec in oxygen-rich silicon, $D_L \approx 2 \times 10^{-14} cm^2/sec$ in oxygen-lean silicon. The recovery speed for all lithium cells (except the Sb-doped cells) has been found to be linearly related to the product of $D_L\ dN_L/dw$. Full room-temperature recovery and the start of redegradation in oxygen-lean lithium cells was usually observed only after several days. Thus, the full dynamic cycle of the crucible cells at room temperature probably encompasses several thousand days. Assuming a cell temperature in orbit of $\approx 50°C$, the time scale for crucible cell dynamics would be compressed by a factor

of ≈ 20 since the activation energy for crucible cell recovery is 1.1 eV. At such temperature, and under the low electron fluxes ($\sim 10^{12}$ e/cm^2 day) in earth orbit, QC cell recovery should keep pace with radiation damage (Ref. 11). Thus, the QC cell would be the proper choice in view of its higher initial performance and greater stability. The minimum lithium gradient compatible with the required recovery speed (which is probably $< 10^{19}$ cm^{-4}, but would depend upon the particle flux level) should be chosen and antimony (initial dopant) should be avoided. The present state-of-the-art in QC (Li) cells should be sufficient to make them superior to 10 ohm-cm n/p cells above about 40° C provided the good stability and the competitive advantage observed under heavy particle irradiation in the laboratory (Ref. 4) is maintained in the space environment.

For lower cell temperatures ($\lesssim 30°C$), the recovery rate of all but heavily doped ($\gtrsim 5 \times 10^{19}$cm^{-4}) QC cells is probably too slow to keep pace with the damaging environment. Under such circumstances oxygen-lean cells would be required. This creates three problems: (1) only a small fraction of the oxygen-lean cells had competitive initial powers, (2) only three cell groups T2(1), H7(1), and T6(1) have stabilized at powers competitive with the n/p levels, and (3) no fully reliable criterion, or set of criteria, for cell stability has been found. On the positive side: (1) oxygen-lean lithium cells have been shown (Ref. 4) to be significantly more radiation resistant to high energy protons and neutrons than n/p cells in laboratory experiments, (2) in most cells, stabilization of photovoltaic response occurs after a period of post-recovery redegradation, and (3) one reasonably good criterion for minimal redegradation, namely, low dN_L/dw, ($< 10^{19}$cm^{-4}) has been found. On the basis of RCA's work to date, the following approaches to improving oxygen-lean cells are suggested: (1) use Lopex rather than float-zone silicons: both RCA's (limited) sampling and the work at Centralab (Ref. 8) show Lopex to produce better cells, (2) aim for low density gradients ($\lesssim 10^{19}$cm^{-4}); this can be achieved by long ($\gtrsim 90$ minutes) redistribution times after a normal (400°C to 425°C) diffusion cycle and also by long, low temperature diffusions, such as the 8-hour, 325°C diffusion, with no redistribution, and (3) use lower starting resistivity: this is extremely important when low lithium density gradients are expected: a starting resistivity of greater than 10 ohm-cm coupled with a low lithium gradient will result in severe series resistance problems and consequent low power factor.

A mission where oxygen-lean lithium cells may offer large benefits would be one where the solar cell temperature would be in the $\sim 240°K$ to 280°K range. At 240°K the recovery rate of oxygen-lean cells (extrapolating on a 0.66 eV activation energy at 240°K) is comparable to the QC cell recovery rate at room temperature. The 280°K recovery rate is ≈ 0.1 that of the oxygen-lean cell room temperature rate which would be more than sufficient for space radiation environments, while the lower temperature would result in longer stability times.

SECTION VI
HALL AND RESISTIVITY MEASUREMENTS

A. INTRODUCTION

The objectives of the Hall and resistivity measurements on bulk-silicon samples diffused with lithium are (1) to determine the dependence of carrier-removal on lithium concentration, oxygen concentration, and electron fluences at low and high bombardment temperatures, and (2) to determine the dependence of annealing at room temperature on the same parameters as in (1). To achieve these objectives, ingots of high-resistivity float-zone (FZ) refined silicon, Monex, and quartz-crucible (QC) grown silicon were procured and are presently being fabricated into Hall bars. Measurements on Hall samples fabricated from silicon procured during the last contract period (Ref. 9) were irradiated and measured. These results will be presented in this report. A complete description of the methods and techniques of these measurements can be found in Reference 9.

B. CARRIER-REMOVAL RATES

The temperature dependence of the carrier-removal rate was measured on four Hall bar samples fabricated from quartz-crucible grown silicon with an initial resistivity $\geq$50 ohm-cm. All samples were irradiated at several bombardment temperatures (T_B), and then the rate of carrier-removal was determined after each bombardment (measurement temperatures, T_M, always being in the range of 78°K to 81°K). These samples were doped with lithium to a concentration of 2×10^{15} Li/cm^3. This data was required to complement RCA's previous data (Ref. 13) obtained on four samples of quartz-crucible silicon doped with lithium to a concentration of 2×10^{16} Li/cm^3. The program objectives of the carrier-removal measurements were completed with the acquisition of these results. These results are shown in Figure 11 where the rates of carrier-removal versus temperature for the lightly doped samples are labeled as curve II, and curve I is the previously reported data of Reference 13. The shift along the temperature axis of curve II relative to curve I is again in agreement with the interstitial-vacancy-close-pair model (Ref. 14) which predicts this shift with changing resistivity. It appears that the saturated value of $\Delta n/\Delta \phi$ cm^{-1} increased with decreasing lithium concentration. This is in contrast to the decrease of $\Delta n/\Delta \phi$ (cm^{-1}) observed (Ref. 9) on float-zone samples as the lithium concentration decreased.

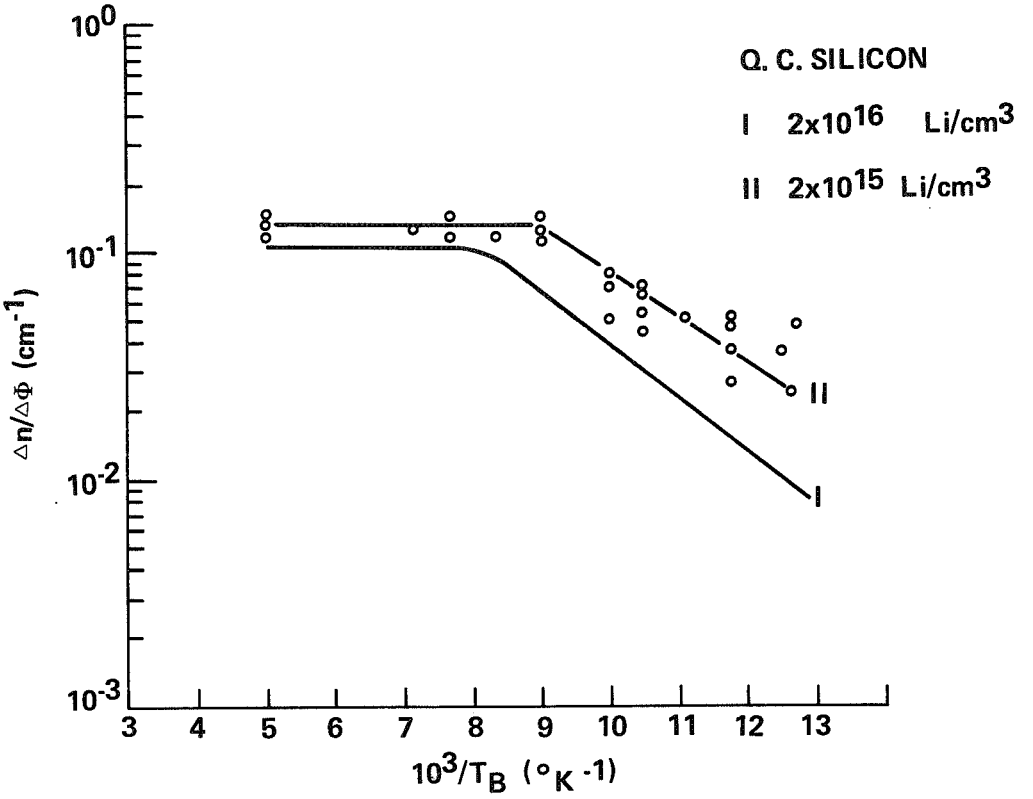

Figure 11. Carrier-Removal Rates vs Reciprocal Bombardment Temperature for Quartz-Crucible Silicon (Measurements at 79°K after Annealing to 200°K)

C. CARRIER DENSITY CHANGES

The carrier density was measured as a function of temperature before bombardment, after bombardment, and following annealing cycles at temperatures of 300°K and 373°K. Figure 12 shows the results obtained on one of the samples which was annealed only at T_A = 300°K. A defect level located at an energy of E_c-0.19 eV is shown in the data of curve II obtained on the sample immediately after bombardment. There is a slight indication that a second shallower level ($\approx E_c$-0.13 eV) is also present. Curve III illustrates the behavior after annealing at a temperature of T_A = 300°K for 36 days. The defect density decreased slightly and the energy of the level did not change significantly from the value calculated before the annealing cycle took place. It should be noted that the carrier density measured at room temperature decreased during the annealing cycle, but the carrier density measured at low temperatures increased. This behavior has been consistently observed on $\approx$14 samples of lithium containing lithium. The significance of these results are discussed in Section VII.

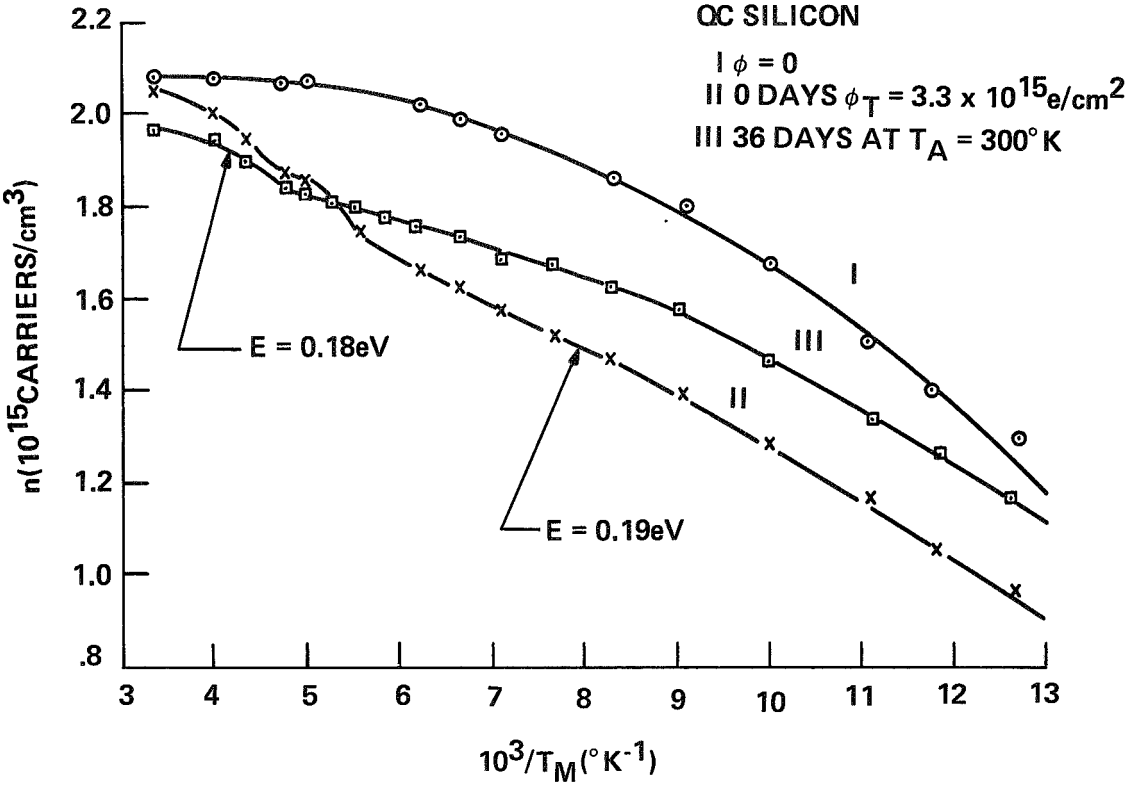

Figure 12. Carrier Density vs Reciprocal Measurement Temperature for Quartz-Crucible Silicon

Figure 13 is a similar set of curves obtained on another sample which differs from Figure 12 in that this sample was first annealed for a short period of time at 100°C and then at room temperature for 54 days. Curve I is based on the initial values of carrier density, curve II was obtained on the sample immediately after bombardment, curve III was obtained following the 100°C annealing cycle, and curve IV was measured after the sample annealed at room temperature. Here again, a defect level located at an energy of E_c-0.16 eV was measured immediately after bombardment and is shown in Figure 13 as curve II. There is some evidence that a second shallower level also exists. This second level is more prominently shown in curve III after completion of the 100°C annealing process at an energy of E_c-0.13 eV where the energy of the first level was calculated to be E_c-0.18 eV. It should be noted that the carrier density decrease measured at T_M = 300°K and the increase measured at $T_M \leq 160$°K agrees with the results of Figure 12.

D. LONG TERM ANNEALING PROCESSES

During this reporting period, several samples of float-zone silicon, which were reported on previously (Ref. 3, 9), were remeasured. Sample H5-5 (1.3 x 10^{16} Li/cm^3)

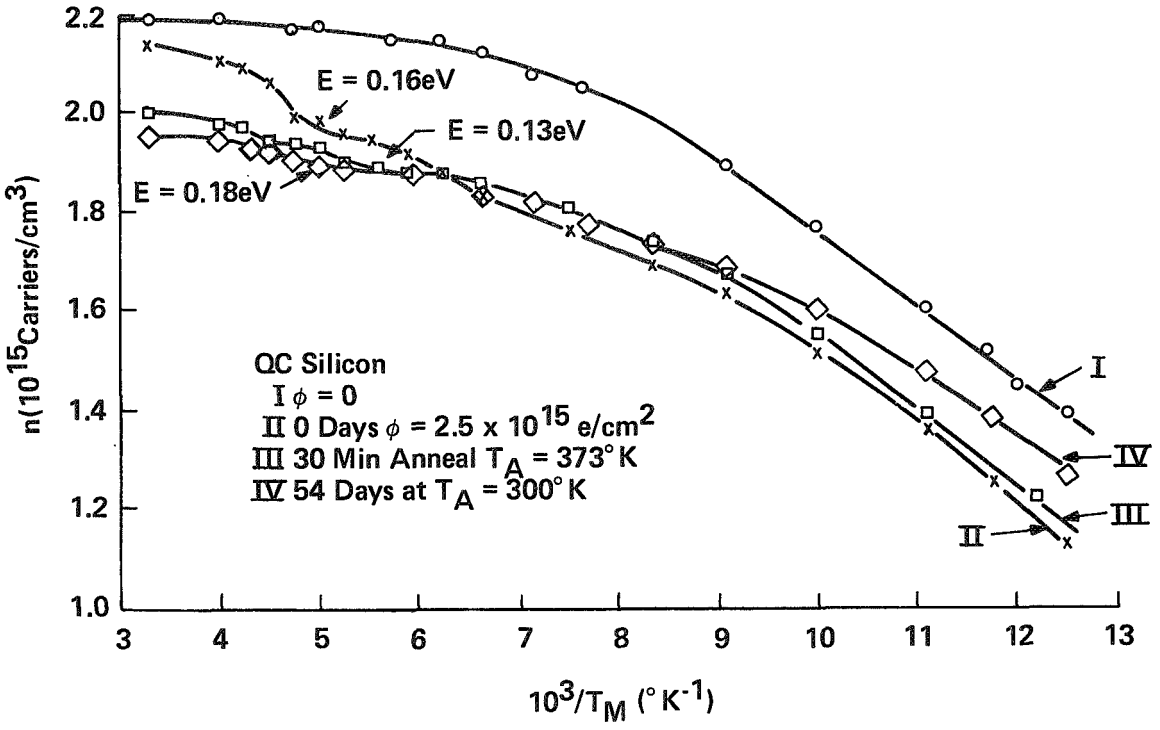

Figure 13. Carrier Density vs Reciprocal Measurement Temperature for Quartz-Crucible Silicon

from Reference 3, showed that the carrier density measured (8 months after bombardment) at $T_M = 300°K$ and at $T_M \approx 80°K$ had not changed from the previous values. This was also true for the values of mobility. Thus, carrier density and mobility values had stabilized for this period of time. In contrast to this behavior, samples of "J" and "H" high resistivity silicon from Reference 9 were remeasured, and the results indicated that the carrier density measured (5 months after bombardment) at low and high temperature were still decreasing as measured previously (Ref. 9). The value of mobility had not changed from the fully recovered value shown in Figure 13 of Reference 9 for a "J" sample, and the mobility recovery of an "H" sample shown in Figure 12 of Reference 9 was still in process. Thus, these high resistivity samples are still in a dynamic state of change.

E. DISCUSSION OF RESULTS

1. Carrier Removal

The dependence of carrier removal on the bombardment temperature and the resistivity of the sample was investigated during the past year. Results obtained on

float-zone silicon previously reported (Ref. 5), and the results presented here are in agreement with the vacancy-interstitial close-pair model (Ref. 14). This model does not include an explanation for the dependence of the saturated value of $(\Delta n/\Delta \phi\, cm^{-1})_{SAT}$ on the resistivity of the samples. The dependence of $(\Delta n/\Delta \phi\, cm^{-1})_{SAT}$ on the lithium concentration appears to be different in samples fabricated from float-zone silicon compared to quartz-crucible silicon. It was shown in Figure 11, and also in Figure 8 of Reference 5, that the rate of carrier removal $(\Delta n/\Delta \phi\, cm^{-1})_{SAT}$ measured on float-zone silicon increased with increasing concentration of lithium and decreased with increasing concentration of lithium. This result obtained on float-zone silicon is in agreement with the experimental results of other workers (Ref. 15); however, the result obtained on quartz-crucible silicon is not. It appears that by increasing the lithium concentration more of the oxygen is tied up by the lithium and is unavailable for the production of A-centers. Since the A-center is the dominant damage center (Ref. 13), the rate of carrier-removal is reduced.

2. Carrier Density Changes

The results shown in Figures 12 and 13 clearly show that at least one and possibly two defects located at $\approx E_c$ - 0.18 eV and $\approx E_c$ - 0.13 eV are introduced during bombardment of lithium-containing quartz-crucible silicon. The defect located at E_c - 0.18 eV is most likely the A-center. A defect level located at E_c - 0.12 eV was observed (Ref. 9) in float-zone silicon of high resistivity. It was conjectured (Ref. 9) that this level is the LiOV on L2 center. This may be the same level shown in Figures 12 and 13.

It was pointed out that the carrier density measured at $T_M = 300°K$ decreased during annealing cycles at $T_A = 300°K$ and the carrier density measured at $T_M \approx 80°K$ increased during this time as shown in Figures 12 and 13. This effect has been observed in measurements that were made on ≈ 14 samples of quartz-crucible silicon doped with lithium to concentrations from 2×10^{15} to 2×10^{16} Li/cm^3. If a single lithium donor neutralizes a single defect (OV^- or $LiOV^-$), then the net change of carrier density is zero. Assuming that two lithium donors are required to neutralize a single defect implies that a decrease in carrier density should be measured at low temperature. Neither one of these explanations agree with the experimental results. A decrease in carrier density was observed (Ref. 13) only on samples which had been annealed at high temperature (e.g., 373°K). In this situation, the loss of donor density was severe. The same condition is achieved by a high level of damage when the electron fluence is approximately equal to or exceeds the lithium concentration (bombardment temperature $\geqq 200°K$). It appears that a stepwise process occurs in which a single lithium neutralizes the defect and then additional complexing of lithium with the neutralized defect occurs. Simultaneous with the first process, there must also be some other competing mechanism or mechanisms, since a single lithium ion complexing with a defect will not produce any net change in carrier-density. The time dependence of this multiple complexing process was illustrated in a previous report (Ref. 9), and

it is shown again as Figure 14 in this report. Clearly the carrier density measured at T_M = 78°K increased over the first 10 days following the bombardment, and then it decreased together with the carrier-density measured at T_M = 300°K. It should be noted that the fluence of $\phi_T = 10^{17}$ e/cm^2, which appears in the legend of Figure 14, is the total fluence accumulated during several bombardments carried out at several bombardment temperatures ranging from 78°K to 200°K. Thus, the fluence at high temperature, namely 200°K was not sufficient to severely deplete the lithium density. This explanation for the gain or loss of carriers in quartz-crucible samples as a function of time after bombardment also agrees with the results obtained on high resistivity float-zone samples of silicon as shown in a previous report (Ref. 9).

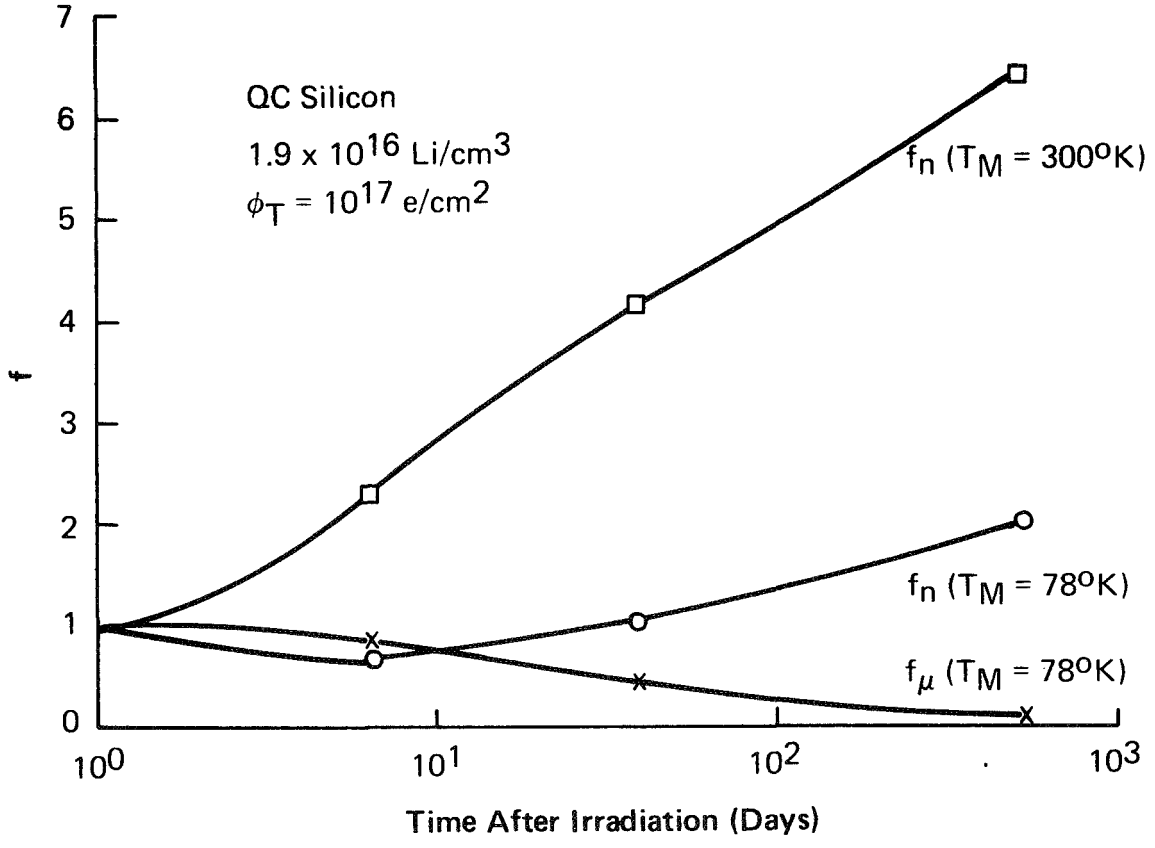

Figure 14. Unannealed Fraction of Carrier Density and Reciprocal Mobility vs Time After Irradiation for 0.3 ohm-cm Quartz-Crucible Silicon (Annealed at T_A = 300°K and Measured at T_M = 78°K and 300°K)

SECTION VII
CONCLUSIONS AND FUTURE WORK

A. GENERAL

Some overall conclusions of the present reporting period are as follows. Information obtained from solar cell experiments has made it possible to formulate a set of design rules and to construct a matrix table listing solar cell parameters and their interrelations. These parameters were divided into three categories (1) fabrication, (2) initial cell parameters, and (3) dynamic and stability parameters. A fourth set of parameters, namely the flight environment, also affects the dynamic and stability parameters. Environmental conditions such as temperature, particle flux, energy, and type of particle must ultimately be considered.

The measurements of Hall bars fabricated from quartz-crucible and float-zone silicon doped with lithium from 2×10^{14} to 2×10^{16} Li/cm^3 have proved successful. These measurements have provided the data required to formulate a qualitative description of the damage and annealing mechanisms that take place in the lithium-oxygen-defect-complex in silicon irradiated by 1-MeV electrons. The model agrees very well with the careful measurements of material parameters which have been made, in a coordinated manner, on practical, JPL-furnished solar cells. Such parameters as minority-carrier diffusion length, lithium-ion probability, spectral response and donor concentrations allowed correlation of effects in solar cells and bulk samples.

B. SOLAR CELL EXPERIMENTS

Performance and stability tests have been run at room temperature for periods ranging up to 550 days on p/n lithium cells and non-lithium n/p control cells irradiated by 1 MeV electrons. Cold finger experiments have been performed to obtain information on lifetime damage constants over a bombardment temperature range from 80° K to 380 °K and on cell recovery dynamics over an annealing temperature range from 280 °K to 380 °K. These experiments have led to the following conclusions on lithium cell properties.

1. Initial Properties

A large fraction of the crucible grown cells had initial powers competitive with the commercial n/p cells. This was true for only a small fraction of oxygen-lean (float-zone and Lopex) cells.

The pre-irradiation lithium donor density gradient, dN_L/dw, provides a good index of the lithium density distribution near the junction and of the dynamic behavior of cell

electrical characteristics after irradiation. Initial cell powers generally decrease with increasing dN_L/dw.

2. Damage Constant

The lifetime damage constant is a factor of ≈ 5 higher in oxygen-lean lithium cells than in crucible (Li) cells.

The damage constant is not strongly dependent on lithium density, changing less than a factor of 2 over a lithium gradient range of ≈ 30.

3. Cell Recovery

Unexpectedly, a significant (≈ 8 percent) n/p cell recovery was observed after irradiation. The contrasting behavior of the slowly recovering crucible cells and the rapidly recovering oxygen-lean cells is due to the $\sim 10^3$ difference in lithium diffusion constant, D_L.

For a given lithium cell type, the recovery speed is proportional to dN_L/dw. Thus, for lithium cells in general (except perhaps cells with antimony-doping), recovery speed is proportional to $D_L dN_L/dw$.

Crucible cells have ≈ 1.1 eV activation energy for recovery; oxygen-lean cells, ≈ 0.66 eV. These are the activation energies for diffusion of lithium in crucible and oxygen-lean silicon, respectively.

4. Cell Stability

Crucible cells have been stable at room temperature, i.e., no redegradation has been observed. The post-recovery powers in most of the crucible cells are competitive with the powers of the recovered n/p cells.

Most of the oxygen-lean cells have suffered some form of instability, either post-recovery redegradation or instability independent of irradiation. The post-recovery short-circuit current redegradation was the most common instability. However, cells which suffered this instability did stabilize after a ≈ 100 day redegradation period, a few of the cell groups stabilizing at powers competitive with similarly irradiated (and recovered) n/p cells. A radiation independent open-circuit voltage instability was suffered by cells of lot C4. This loss, which is due to carrier loss in the base region has occurred continuously over ≈ 500 days.

The quantity dN_L/dw is one good index for predicting cell stability. Cells with low dN_L/dw are usually more stable then cells with high dN_L/dw.

In cells with low dN_L/dw and high starting resistivity (>20 ohm-cm), significant series-resistance problems are encountered. This probably could be avoided by employing starting resistivities of $\lesssim 10$ ohm-cm.

The work to date has led to the following conclusions on the mission possibilities for lithium cells:

(a) Crucible cells would be compatible with missions in which cell temperatures are $\geq 40^\circ$ C. The recovery rate at these elevated temperatures should be sufficient to keep pace with the electron flux ($\sim 10^{12}$ 3/cm^2 day) experienced in earth orbit. The present state-of-the-art should be sufficient to give them an advantage over n/p cells if the good stability and the competitive advantage observed under heavy particle irradiation in the laboratory is maintained in the space environment.

(b) Oxygen-lean cells show promise for missions where cell temperatures are low, i.e., $\sim 280^\circ$ K. However, additional work will be required to improve the initial performance and stability of these cells.

C. LITHIUM DIFFUSION CONSTANT

The lithium diffusion constant measurements have shown that, as previously found with other cells, the recovery of high density gradient quartz - crucible cells is associated with the diffusion of free lithium (Li^+). The diffusion constants of the high density gradient cells, C5-19 and C5-20, show excellent agreement with the published data of Pell, unlike the previous results on lower density gradient cells (C6C-20-dN_D/dw = 2×10^{18}/cm^4) (Ref. 9). The conclusion is, thus, that the conventional diffusion of ions is not impaired by the presence of high lithium density gradients (5×10^{19}/cm^4).

D. HALL MEASUREMENTS

In agreement with previous results (Ref. 13), defects located at an energy of $\approx E_C$ - 0.18 eV and $\approx E_C$ - 0.13 eV were measured in quartz-crucible silicon of moderate resistivity (2×10^{15} Li/cm^3) bombarded by electrons at temperatures from 78° K to 200° K. Both of these defects anneal at room temperature by the interaction of lithium with the defects. These defects would only influence the electrical characteristics of solar cells operating at room temperature if the lithium concentration in the cell was adjusted so as to locate the Fermi level within 2 kT of the defect energy level.

The rate of carrier-removal $(\Delta n/\Delta \phi \text{ cm}^{-1})_{SAT}$ appears to increase with decreasing lithium concentration. This suggests that the lithium combined with oxygen so as to limit

the oxygen concentration available for A-center formation and the introduction rate of the LiOV center is lower than the A-center introduction rate. This explanation agrees with the conclusions of Reference 9 based on the results obtained on high resistivity (10 to 20 ohm-cm) float-zone silicon.

Annealing results obtained on the quartz-crucible Hall bars suggest that several competing processes take place during the post-bombardment period. The short-term experimental results cannot be explained on the basis of a single or a double lithium ion neutralizing a defect. Over a long period of time following bombardment, the results can be explained as due to a multiple complexing by many lithium ions at a defect center so as to produce an unchanged complex.

The experimental results of this and previous responds (Ref. 3, 5, 9) suggest that the previously reported (Ref. 16) radiation damage and annealing model be modified to explain these results. It is suggested that the dominant damage center in low-resistivity float-zone silicon (10^{15} to 10^{16} Li/cm^3) is the L1 center which is described by Equation (1):

$$Li^+ + V \rightleftharpoons LiV^- \quad \left[\text{L1-center}\right] \tag{1}$$

One of the observed (Ref. 13) annealing mechanisms is the dissociation of the L1 center, thus Equation (1) is written with a double arrow indicating that an equilibrium exists between the formation of the defect center and the dissociation of this center. In addition to the dissociative mechanism of annealing, there is the mechanism of neutralization by which lithium complexes with the L1 center. This process is described by Equation (2).

$$LiV^- + Li^+ \rightleftharpoons Li_2V \quad \left[\text{annealed L1 center}\right] \tag{2}$$

Equation (2) is written with a double arrow so as to indicate that the annealed L1 center is unstable and the reaction can proceed in the reverse direction. The redegradation is caused by this reverse process (see Ref. 5).

The dominant damage center in high resistivity (5×10^{14} Li/cm^3) float-zone silicon appears to be the L2 center which is given by Equation (3):

$$LiO^+ + V^= \rightleftharpoons LiOV^- \quad \left[\text{L2-center}\right] \tag{3}$$

The annealing of the L2 center takes place by means of the mechanism of neutralization described by Equation (4):

$$LiOV^- + Li^+ \longrightarrow Li_2OV \quad \left[\text{annealed L2 center}\right] \tag{4}$$

In quartz-crucible silicon, the dominant center (Ref. 13) appears to be the A-center for samples with lithium concentrations from 10^{15} to 2 x 10^{16} Li/cm^3. The formation of the A-center is described by Equation (5):

$$O + V^{=} \longrightarrow OV^{-} \left[\text{A-center}\right] \tag{5}$$

For the samples with higher lithium concentrations or samples bombarded by higher fluences, the production of the L1 and L2 centers will contribute to the total damage. It is necessary to postulate that lithium continues to complex with annealed defect centers during the post-irradiation period of annealing since RCA's results (see Ref. 9) showed that the mobility recovered as a function of annealing time, but the carrier density continued to decrease at the same time. Thus, a possible mechanism is given by Equation (6):

$$Li^{+} + OV^{-} \left[\text{A-center}\right] \longrightarrow e + Li_2OV \left[\text{annealed L2 center}\right] + Li_{n-2}^{+} \rightarrow Li_nOV \tag{6}$$

where the subscript n indicates that more than one lithium ion can complex with the annealed A-center. This mechanism will also apply to the neutralization of the L2 center as given by Equation (7):

$$LiOV^{-} \left[\text{L2-center}\right] + Li^{+} \rightarrow e + Li_2OV \left[\text{annealed L2 center}\right] + Li_{n-2}^{+} \rightarrow Li_nOV \tag{7}$$

Equations (4), (6), and (7) will be modified by competing single and double lithium-ion interactions as explained in the discussion (see Figures 12, 13, and 14). In addition, some unknown annealing processes must also compete since any combination of single and double processes cannot explain the increase of carrier density (T_M = 78° K) during room temperature annealing of quartz-crucible samples. In contrast to this conclusion, the results obtained on the high-resistivity (10 to 20 ohm-cm) float-zone silicon (Ref. 5, 9) can be explained only by a multiple lithium ion process described by Equation (7) where the intermediate single lithium process is omitted.

E. FUTURE PLANS

1. Solar Cell Studies

Stability tests will be continued. Investigations into variations in initial parameters within given cell lots and their correlation with cell dynamics after irradiation will be continued. The tests will be guided by the matrix of cell samples recommended in this report.

2. Hall Measurements

The contract calls for the termination of Hall measurements with the completion of this Quarterly Report. All of the future efforts will be concentrated on solar cell tests.

REFERENCES

1. J. Hilibrand and R. D. Gold, RCA Rev. 21, 245 (1960).

2. W. Rosenzweig, Bell Sys. Tech. Journ., 41, 1573 (1960).

3. G. J. Brucker, T. J. Faith, J. P. Corra, and A. G. Holmes-Siedle, First Quarterly Report, JPL Contract No. 952555, prepared by RCA and issued October 10, 1969.

4. T. J. Faith, G. J. Brucker, A. G. Holmes-Siedle, and J. Wysocki, Proc. Seventh Photovoltaic Spec. Conf., IEEE Catalog No. 68C63ED, 131 (1968).

5. G. J. Brucker, T. J. Faith, J. P. Corra, and A. Holmes-Siedle, Second Quarterly Report, JPL Contract No. 952555, prepared by RCA and issued Jan. 10, 1970.

6. E. M. Pell, J. Appl. Phys. 31, 291 (1960).

7. E. M. Pell, Phys, Rev. 119, 1222 (1960).

8. E. M. Pell, J. Appl. Phys. 32, 6 (1961).

9. G. J. Brucker, T. J. Faith, J. P. Corra, and A. Holmes-Siedle, Third Quarterly Report, JPL Contract No. 952555, prepared by RCA and issued April 10, 1970.

10. F. J. Morin and J. P. Maita, Phys. Rev. 96, 28 (1954).

11. D. L. Reynard and D. B. Orvis, Proc. Seventh Photovoltaic Spec. Conf., IEEE Catalog No. 68C63ED, 108 (1968).

12. P. A. Iles, Proc. Seventh Photovoltaic Spec. Conf., IEEE Catalog No. 68C63ED, 117 (1968).

13. G. J. Brucker, Phys. Rev. 183, 712 (1969).

14. F. L. Vook and H. J. Stein, "Products of Defects in N-Type Silicon, "Proceedings of the Santa Fe Conference on Radiation Effects in Semiconductors, Plenen Press, N. Y., pp 99-114, Oct. 1967.

15. H. J. Stein and R. Gereth, J. Appl. Phys. Vol. 39, pp 2890, 1968.

16. G. J. Brucker, T. J. Faith, and A. G. Holmes-Siedle, Final Report, JPL Contract No. 952249 prepared by RCA and issued April 21, 1969.

RCA | Defense Electronic Products | Astro Electronics Division | Princeton, New Jersey